Inorganic Chemistry

pubs.acs.org/IC

Article

Acoustic Shock Wave-Induced Rutile to Anatase Phase Transition of TiO_2 Nanoparticles and Exploration of Their Unconventional Thermodynamic Structural Transition Path of Crystallization Behaviors

Sivakumar Aswathappa, Lidong Dai,* Sahaya Jude Dhas Sathiyadhas, Raju Suresh Kumar, and Mowlika Varadhappa Reddy

Cite This: *Inorg. Chem.* 2024, 63, 17043−17055

Read Online

ACCESS | Metrics & More | Article Recommendations | Supporting Information

ABSTRACT: Titanium dioxide (TiO_2) is one of the most well-known and long-standing polymorphic materials in the transition metal oxide group of materials. The transition from rutile to anatase is one of the long-standing fundamental questions among materials science researchers because seeking the nucleation site at the beginning of the phase transition is highly challenging. Until now, there have been no studies on the unconventional structural phase transition of TiO_2 nanoparticles by acoustic shock waves. In the present study, this work provides the first evidence on the solid-state nanostructure of the rutile-to-anatase phase transition of TiO_2 by acoustic shock waves whereby these phase transition results are evaluated by Raman spectroscopy, thermal calorimetry, X-ray photoelectron spectroscopy, and microscopic techniques. We propose a novel mechanism for the occurrence of the rutile-to-anatase phase transition based on thermophysical properties and shock wave-induced melting concepts. Under shocked conditions, the R−A phase transition occurs because of the anatase phase's lower interfacial energy ($\gamma^{L/A}$) and surface energy compared to rutile. We strongly believe that the present work can provide in-depth insight into understanding the crystallization concepts of the TiO_2 NPs under extreme conditions, especially with regard to the rutile-to-anatase phase transition.

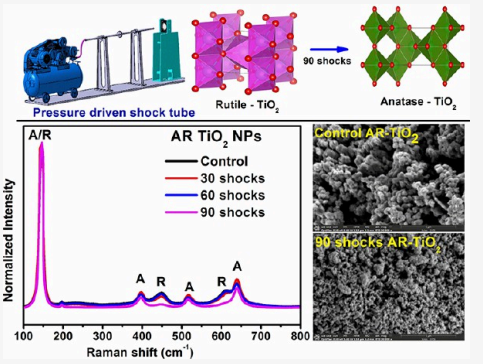

INTRODUCTION

Titanium dioxide is one of the pioneering polymorphic and chemistry-rich compounds, like silicon dioxide, because of its multiple oxidation states arising out of the partially filled *3d* shell, and such materials of prominence always have a high degree of research interest in high-pressure science domains, which include materials science and geological sciences.[1−3] Over the past few decades, researchers of high pressure/temperature have made significant contributions to understanding the polymorphic and stoichiometry changes of TiO_2 with respect to the external conditions experimentally[4] as well as theoretically[5] and thereby found several interesting phase transition paths and crystallization behaviors. From the literature, it can be found that TiO_2 can be crystallized in several crystallographic phases such as rutile ($P4_2/mnm$), anatase ($I4_1/amd$), brookite ($Pbca$), TiO_2-B ($C2/m$), TiO_2-R ($Pbnm$), TiO_2-H ($I4/m$), pyrite ($Pa\text{-}3$), columbite ($Pbcn$), baddeleyite ($P21/c$), cotunnite, α-PbO_2 type TiO_2 (TiO_2-II), fluorite ($Fm3\text{-}m$), cubic, and post cotunnite phases.[6−9] Among the above-listed phases, naturally existing polymorphs are rutile, anatase, brookite, and TiO_2-B while the remaining phases are considered as high pressure polymorphs which can be obtained under extreme conditions.[6−9] It is worth mentioning that among the four most common polymorphs, rutile is the most stable phase, followed by anatase, brookite, and TiO_2-B, whereas at the nanoscale region (the critical particle size is 10 nm), the anatase phase becomes the most thermodynamically stable phase compared to rutile.[10,11] Most of the common forms of anatase and rutile TiO_2 have technological applications on the basis of their nanoscale morphologies and crystallographic structures. The relationship between the TiO_2 phases, their relative stability of interconversion, and the structure−property relationship has been particularly well-studied for bulk and nanocrystals.[12,13]

The anatase and rutile phases have different structural evolutions under static (steady-state thermodynamical conditions−diamond anvil cell)[14,15] and dynamic (unsteady state thermodynamical conditions−shock waves)[16−18] high pressure/temperature conditions while the critical pressure/

Received: July 1, 2024
Revised: August 20, 2024
Accepted: August 23, 2024
Published: August 29, 2024

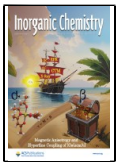

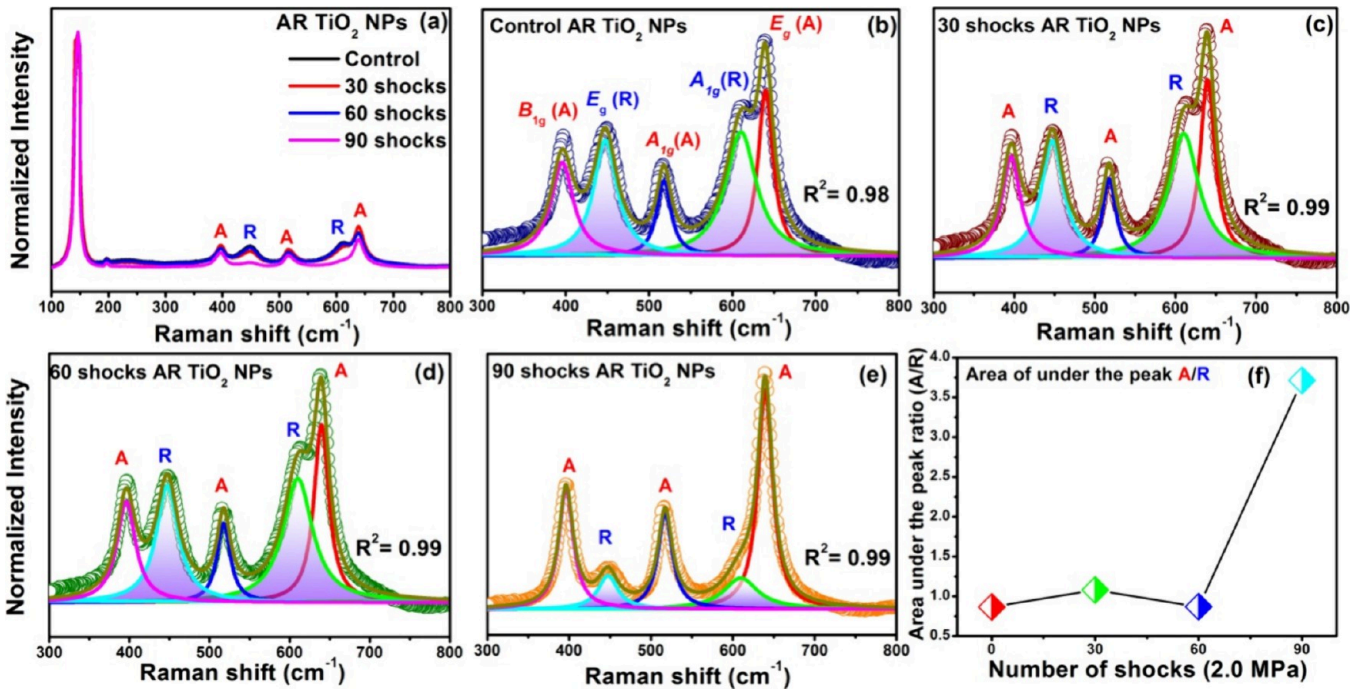

Figure 1. Raman spectral features of the control and shocked AR TiO_2 NPs. (a) Recorded Raman spectra over the wavenumber region 100−800 cm^{-1}. (b−e) Internal Raman bands of the (b) control sample, (c) 30-shocked sample, (d) 60-shocked sample, and (e) 90-shocked sample. (f) Area under the peaks' ratio of the AR TiO_2 NPs of the Raman bands with respect to the number of shock pulses.

temperature is obviously different for nano and bulk solids.[14−18] For instance, Li et al. reported the nanoporous rutile-to-baddeleyite TiO_2 phase transition at 26.1 GPa by subjecting it to static compression,[19] and the anatase-to-baddeleyite transition is observed at 21 GPa.[20] Wang et al. investigated a similar compression experiment with the mixed phase of anatase/rutile TiO_2 and observed that anatase particles would convert into the amorphous phase and the rutile particles would convert into baddeleyite at 16.4 GPa.[21] Anatase TiO_2 particles follow different phase transition sequences based on their initial particle size as follows: the nanoparticles undergo the anatase-amorphous phase transition under high pressure when the particle size is lower than 10 nm[22−25] whereas this type of direct transition is absent in the case of bulk TiO_2.[25] The anatase-to-baddeleyite transition occurs when the particles' size appears between 12 and 50 nm.[20,24] The anatase−columbite−baddeleyite phase transition occurs when the particles are larger than 50 nm,[24,26] whereas, in the case of the pure static temperature-dependent annealing condition, the anatase to rutile phase transition begins at ∼580 °C and is completed at ∼900 °C[27,28] and the rutile phase remains stable for higher temperatures up to 1200 °C.[29,30] The anatase to rutile phase transition is the most thermodynamically favorable phase transition path for TiO_2 and it is irreversible.[30,31] Under steady-state conditions, according to the thermodynamic properties of anatase and rutile, rutile cannot be converted into the anatase phase because of the absence of any phase equilibrium. This is one of the long-standing fundamental research problems of TiO_2 for researchers cutting across all the science domains. In general, rutile is a thermodynamically stable phase and kinetically favored, which means, under chemical reaction conditions, rutile can easily react with the solutions and undergo structural transitions.

On the other hand, so far, very few articles have been made available in the literature for the rutile-to-anatase transition in chemically doped TiO_2 nanosystems by various techniques such as oxygen plasma immersion ion implantation,[32] under oxygen pressures,[33] contacting the strongly negatively charged colloid particles,[34] chlorination,[35] and ammonolysis[36] and this phase transition occurs because, in strong acidic solutions, the condensation rate is slow enough and the formation of the rutile phase is kinetically favored. In addition, during the femtosecond laser shock wave irradiation on the rutile bulk single crystals, the rutile−anatase transitions were observed on the surface of the crystals.[37−39] To date, no report is available for the thermodynamically converted solid-state rutile-to-anatase transition in nanosystems.

In recent years, mild-acoustic shock wave processing on nanocrystalline materials has become one of the fascinating research problems such that it has linearly grown from the beginning of the 21st century because of its spectacular applications in structural phase transitions and surface modifications.[40,41] Especially, in TiO_2 nanosystems, there has been a considerable number of publications reported using conventional shock tubes[42−44] and tabletop shock tubes.[45,46] For instance, using a conventional shock tube, Jayaram et al. observed the complete anatase-to-rutile transition at 1 pulse shocked condition with the transient pressure of 6.6 MPa,[42] and a mixed phase of anatase and rutile TiO_2 was observed by Kim et al.[43] and Freitas et al.[44] By using the tabletop shock tube, Kalaiarasi et al. reported a complete anatase−rutile transition upon the exposure of 90 shock pulses[45] and Aswathappa et al. also found similar results under the same shocked conditions,[46] whereas the rutile TiO_2 NPs remain in the same crystalline structure even at the 90-shocked condition with a transient pressure of 2.0 MPa.[46] Our research group has already investigated the shock resistance behavior of the mixed phase of brookite/rutile TiO_2 NPs (brookite rich-TiO_2) and

https://doi.org/10.1021/acs.inorgchem.4c02723
Inorg. Chem. 2024, 63, 17043−17055

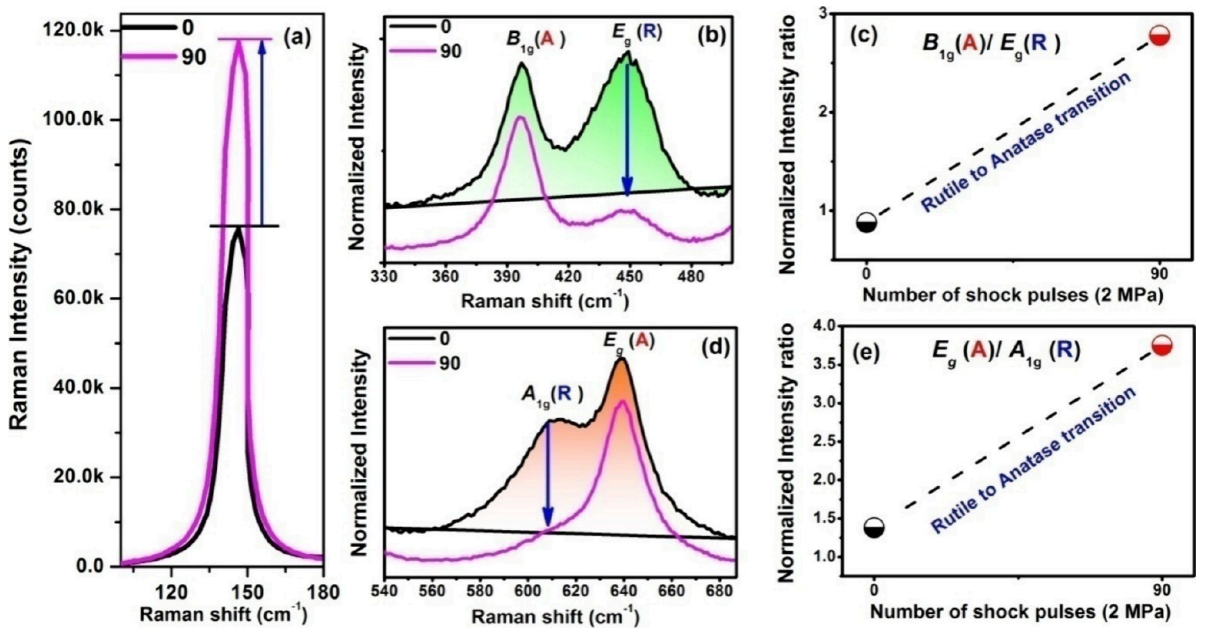

Figure 2. Zoomed-in Raman fingerprint patterns of the control and 90-shocked TiO_2 NPs. (a) E_g mode. (b) Raman bands of the B_{1g} and E_g. (c) Normalized intensity ratio of the B_{1g} and E_g. (d) Raman bands of the A_{1g} and E_g. (e) Normalized intensity ratio of the A_{1g} and E_g.

found the absence of structural transitions even up to 300-shocked conditions.[47]

For the first time in the literature, herein we report the rutile-to-anatase phase transition in nanocrystalline TiO_2 under acoustic shocked conditions, which is essentially not possible in steady-state thermodynamical conditions such as static heating and compression conditions. The present work offers a new possible way to initiate the unconventional thermodynamic structural transition by tabletop shock tube experiments. In the first part, the rutile-to-anatase phase transition is justified by various analytical techniques such as spectroscopic, calorimetric, microscopic, and electron diffraction techniques. In the second part, a novel mechanism is provided for the rutile to anatase phase transition in TiO_2 NPs that is based on its thermophysical properties and shock wave-induced superheating concepts.

EXPERIMENTAL SECTION

Syntheses of TiO_2 Nanostructures. To prepare the TiO_2 solution, 2 mL of titanium(IV) isopropoxide was added to 200 mL of deionized water with continuous magnetic stirring at room temperature. During the precursor solution preparation, 20 mL of glacial acetic acid, serving as a chelating agent, was added dropwise to prevent nucleophilic attacks on the titanium isopropoxide by water. The solution was subsequently heated to 80 °C until the xerogel was completely dried, then allowed to cool naturally to room temperature. The dried gel was ground into a fine powder and then calcinated at 700 °C for 5 h in a muffle furnace.

Shock Wave Loading Experiment. The detailed information on the shock wave loading procedure and analytical instrument details are presented in the Supporting Information. For the present experiment, totally 4 equal samples have been chosen such that one sample has been kept as the control sample while the other three samples have been treated with 30, 60, and 90 shocks with the Mach number of 2.2. Figure S1(a and b) shows the schematic diagram of the experimental setup of the shock tube. Subsequently, 30 shock pulses were loaded on the test sample with an interval of 5 s between each shock pulse. For example, 30 pulses mean shock wave-exposed on a sample 30 times with Mach number 2.2 (±0.1). For the current study, we have chosen shock waves of Mach number 2.2 with a transient pressure (P_5) and temperature (T_5) of 2.0 MPa and 864 K, respectively.

RESULTS AND DISCUSSION

The Rutile-to-Anatase Phase Transition of TiO_2 by the Raman Spectroscopic Results. The recorded Raman spectra of the control and shocked TiO_2 samples are shown in Figure 1a. The control sample has five internal Raman bands at 395, 447, 517, 610, and 639 cm^{-1}, respectively. Among the five Raman bands, the bands at 395 (B_{1g}), 517 (A_{1g}), and 639 cm^{-1} (E_g) belong to the fingerprint Raman bands of the anatase phase[45] and the bands at 447 (E_g) and 610 cm^{-1} (A_{1g}) belong to the Raman bands of the rutile phase.[45] Based on the observed Raman spectral results, the control sample has a mixed phase of anatase and rutile, which occurs because of the lower calcination temperature (700 °C). Under shocked conditions, considerable changes have occurred in the internal and lattice Raman bands with respect to the number of shock pulses, and the corresponding Raman spectra are displayed in Figure 1a. For more clarity of the obtained results, the internal Raman bands of the control, 30, 60, and 90 shock pulse-loaded TiO_2 samples are depicted in Figure 1b−e. Up to 60-shocked conditions, all the anatase Raman bands are retained in their respective Raman shift positions as well as the respective intensity, whereas the rutile Raman band's 610 cm^{-1} (A_{1g}) has experienced a slight reduction in the intensity at the exposure of 30 shocks but regained its intensity at the 60-shocked condition. However, at the exposure of 90 shocks, significant changes occurred such that all of the rutile Raman bands such as 447 (E_g) and 610 cm^{-1} (A_{1g}) experienced significant reduction in their respective intensities (Figure 1e), which clearly demonstrates the occurrence of the rutile-to-anatase phase transition.

The areas under the anatase and rutile internal Raman bands have been calculated with respect to the number of shock pulses, and the corresponding profile is presented in Figure 1f. It is clear that the A/R peak ratio has significantly increased at the exposure of 90 shocks compared to the control and other

https://doi.org/10.1021/acs.inorgchem.4c02723
Inorg. Chem. 2024, 63, 17043−17055

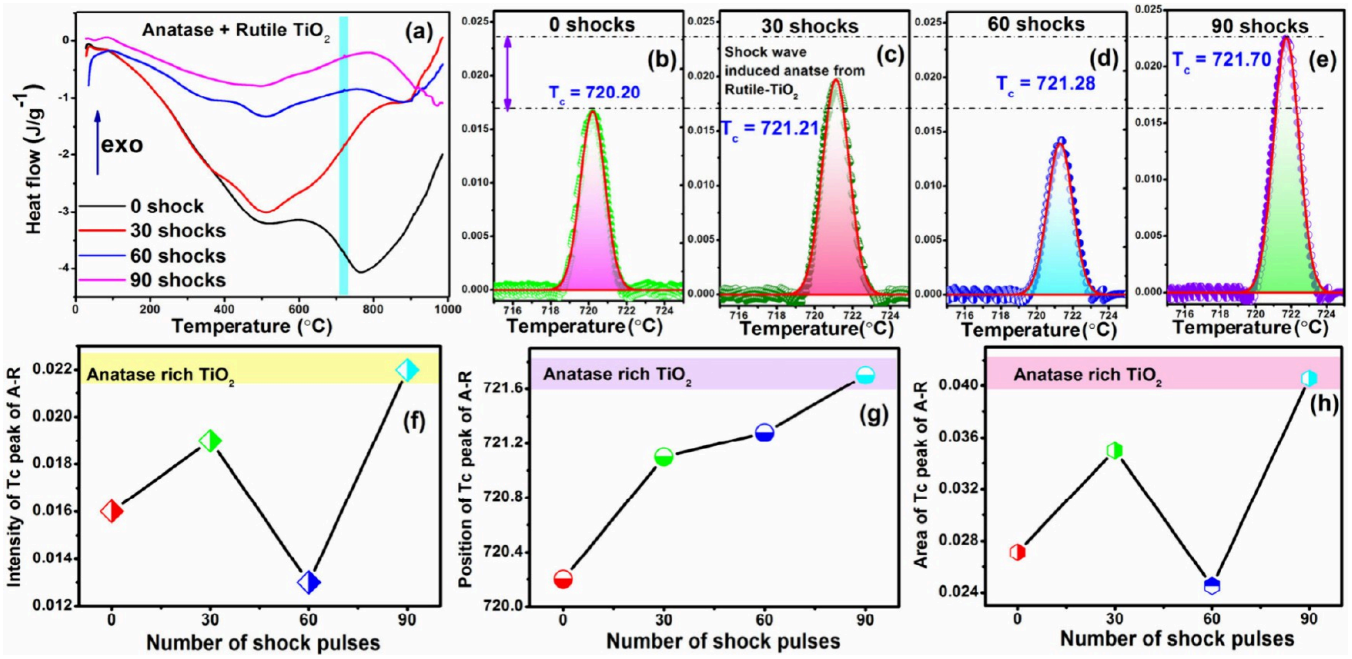

Figure 3. (a) DSC profiles of TiO_2 NPs with respect to the number of shock pulses. (b–e) Zoomed-in portion of the exothermic peak of the control and shocked TiO_2 samples, as well as (f) intensity, (g) position, and (h) area of the exothermic peak with respect to the number of shock pulses.

shocked conditions, which provides direct evidence for the rutile-to-anatase phase transition, and similar kinds of results have been witnessed in the rutile single crystal under femtosecond laser irradiation conditions.[37−39] The Raman band at 143 cm^{-1} (E_g) in the lower wavenumber region also provides convincing testimony for the rutile-to-anatase phase transition or vice versa.[37−39] The E_g Raman band is common for both phases, but it has a very high intensity for the pure anatase and a lower intensity for the pure rutile phase.[37−39]

As shown in Figure 2a, the zoomed-in portion of the lattice mode of the E_g mode is presented without normalization, and it was found that it has higher intensity at the 90-shocked condition compared to the control sample, which very well supports the occurrence of the rutile-to-anatase transition.[37−39] In Figure 2b and c, the internal Raman band features of the anatase and rutile phases [B_{1g} (A) and E_g (R)] are showcased for the control and 90-shocked samples, and it is observed that the E_g (R) mode is found to have been reduced at the 90-shocked condition. The calculated values of the normalized intensity ratio are determined as 0.88 and 2.28, respectively, for the control and the 90-shocked samples. A similar kind of observation has been confirmed in the normalized intensity ratio features of the E_g (A) and A_{1g} (R) Raman modes for the control and 90-shocked samples such that the corresponding profiles are portrayed in Figure 2d and e. Based on the features of Figures 1 and 2, it is obvious that most of the rutile particles have converted into the anatase phase. In summary, the TiO_2 NPs have the mixed phase with the rutile and anatase phases, whereas at the exposure of 90 shocks, the anatase phase particles are found to have increased significantly.

Shock Wave-Induced Anatase Phase Evolution by Thermal Calorimetric Results. In thermal analysis, the appearance of the exothermic peak ∼700 °C is usually considered as a reference of the crystallization point for the demonstration of the anatase-to-rutile phase transition, and its intensity is directly proportional to the anatase−rutile phase conversion quantitatively.[48,49] The recorded DSC profiles of the control and shocked TiO_2 samples are presented in Figure 3a, wherein the appearance of the exothermic peak around the peak at 720 °C is marked in cyan color. As seen in Figure 3a, the intensity of the exothermic peaks is abnormally low, such that their differences could not be observed. Because the control TiO_2 NPs have almost equal percentages of the anatase and rutile phase particles, the rutile particles do not contribute to the exothermic reaction in this region due to their high thermal stability and only the available anatase particles are the major responsible factors for the exothermic peak intensity. So, for better visibility, the zoomed-in profiles of the exothermic peaks of the control and shocked samples are depicted in Figure 3b−e. The intensity of the exothermic peak has experienced considerable changes with respect to the number of shock pulses, and the observed values are determined as 0.016, 0.019, 0.013, and 0.022 for their correspondent 0, 30, 60, and 90 shocks, respectively.

The intensity of the exothermic peak is slightly increased for the 30-shocked sample compared to the control sample, which is probably owing to the conversion of a few rutile particles in to the anatase phase such that the Raman spectral results also provided similar results. However, the intensity of the exothermic peak will be reduced at the 60-shocked condition because of the dominance of the rutile particles. Noteworthily, the exothermic peak has a higher intensity for the 90-shocked sample than others, since it has a higher concentration of the anatase particles, which provides strong evidence for the occurrence of a significant rutile-to-anatase phase transition. The A−R exothermic peak intensity, position, and area with respect to the number of shock pulses are presented in Figure 3f−h, wherein the observed profile data support the formation of the anatase-rich TiO_2 at the 90-shocked condition following up for the rutile-to-anatase phase transition. The inter-relation between the ratio of the A/R Raman bands area and the A-R

https://doi.org/10.1021/acs.inorgchem.4c02723
Inorg. Chem. 2024, 63, 17043−17055

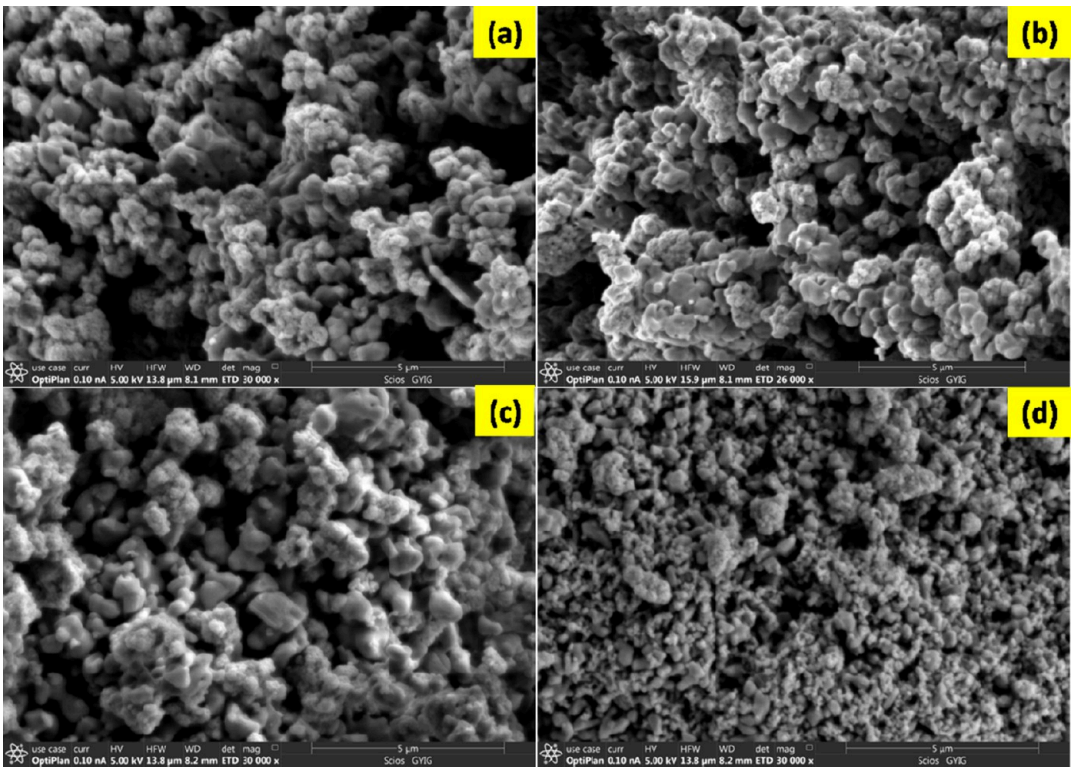

Figure 4. SEM images of the control and shocked TiO_2 NPs. Herein, (a) control; (b) 30-shocked; (c) 60-shocked and (d) 90-shocked TiO_2 NPs, respectively.

exothermic peak intensity is found to be directly proportional (Figure S2).

Shock Wave-Induced Melting and Dynamic Recrystallization of TiO_2 NPs: Microscopic Results. Crystallization of TiO_2 structures such as anatase and rutile is highly sensitive to the particle size, and generally anatase particles crystallize below ∼30 nm while rutile is formed above ∼30 nm.[50−52] In light of the vibrational spectroscopic and thermal calorimetric results, the 90-shocked TiO_2 sample's particle size is reduced significantly due to the rutile-to-anatase phase transition. In general, static heating methods are highly favorable for the increment of particle size due to the grain coarsening effect.[50−52] So, understanding the surface morphological changes and size changes is essential to draw convincing results on the shock wave-induced rutile-to-anatase phase transition in TiO_2 NPs. The captured SEM images of the control and shocked TiO_2 are displayed in Figure 4. The control TiO_2 sample has two sets of particle sizes with different morphologies. The higher size particles belong to the rutile phase, and the ultrasmaller particles belong to the anatase phase. The size distribution of the anatase and rutile TiO_2 NPs could not be analyzed by the SEM images because the anatase has ultralower size particles such that the particle size could not be precisely measured. Under 30 and 60 shocked conditions, the TiO_2 NPs do not experience significant changes from their initial particle size and shapes (Figure 4b and c). However, at the 90-shocked condition, remarkable changes could be clearly witnessed in the particle size changes such that most of the large-size particles have been converted into the downscale of the particles which is due to the occurrence of the rutile-to-anatase phase transition.[50−52] The significant reduction in the particle size at the 90-shocked condition occurs because of the shock wave-induced dynamic recrystallization process, for which the lower thermal conductivity materials are highly favorable.[53−55]

In Figure 5, the features of the TEM images of the control and 90-shocked TiO_2 NPs are observed. It makes clear that the average particle size is ∼48 nm and the rutile particle also belongs to a well-defined hexagonal morphology.

At the 90-shocked condition, the particles of hexagonal morphology are significantly reduced in size such that they are turned into the morphology of nonhexagonal (Figure 5e−h). The lattice fringe patterns of the control TiO_2 sample can be witnessed in Figure 5i−k, wherein the mixed phases of the anatase and rutile particles are observed (Figure 5i). At the 90-shocked condition, the rutile particles' concentration is reduced such that the anatase particles' concentration is increased, and the corresponding lattice fringe patterns are presented in Figure 5l−n. The overall features of the TEM images also evidently support the occurrence of the rutile-to-anatase phase transition at the 90-shocked condition.

In Figure 6a and b, the electron diffraction features of the control and the 90-shocked samples are presented while the zoomed-in portions are portrayed in Figure 6c and d. As displayed in Figure 6c, the anatase (101) and rutile (110) diffraction spots have almost equal intensity, whereas the rutile-diffraction spots' intensity is found to have reduced because of the formation of the anatase-rich TiO_2 resulting from the rutile-to-anatase phase transition (Figure 6d).

Shock Wave-Induced Oxidation State Changes (Ti^{3+} to Ti^{4+}) in TiO_2 NPs: XPS Results. Figure 7 shows the core XPS band features of the TiO_2 NPs, and the survey spectra of the control and 90 shocked TiO_2 NPs are also presented (Figure S3). In the XPS results, a significant difference could not be identified between the anatase and rutile phases of TiO_2 NPs, as it is in the Raman and morphological aspects. Both

https://doi.org/10.1021/acs.inorgchem.4c02723
Inorg. Chem. 2024, 63, 17043−17055

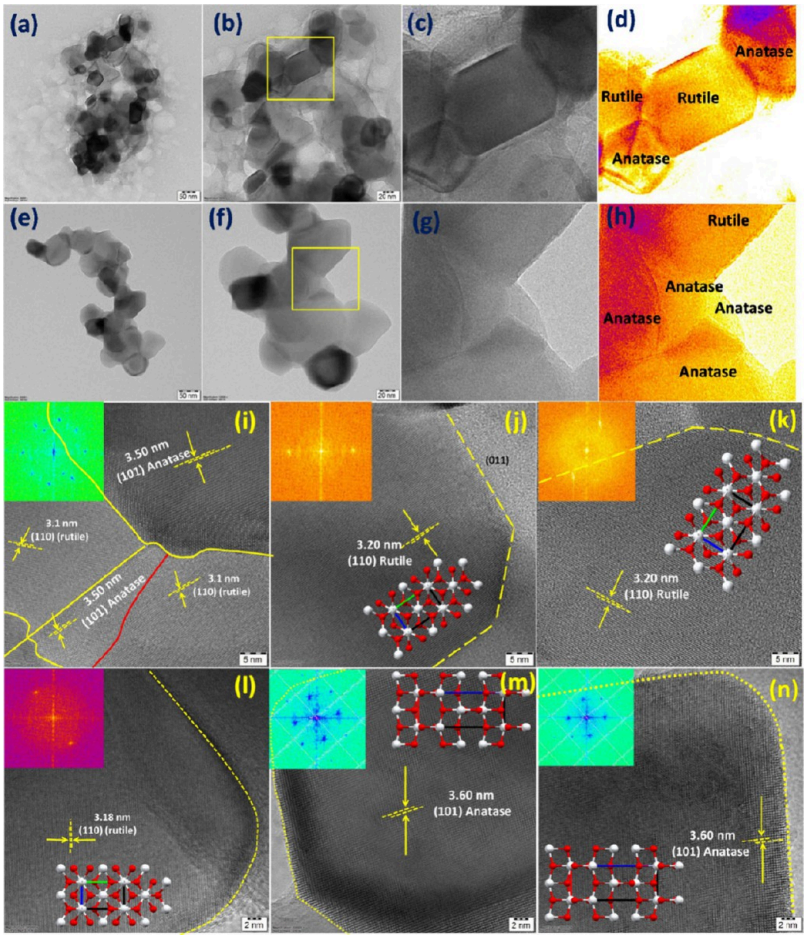

Figure 5. TEM images of the control and 90-shocked TiO_2 NPs. (a–d) TEM images of the control TiO_2 NPs. (e–h) TEM images of the 90-shocked TiO_2 NPs. (i–k) Lattice fringe patterns of the control TiO_2 NPs. (l–n) Lattice fringe patterns of the 90-shocked TiO_2 NPs (insets: FFT patterns).

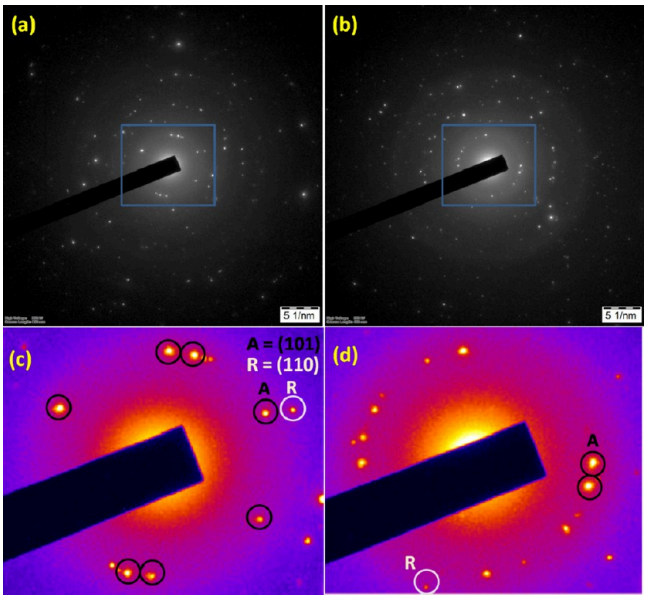

Figure 6. Electron diffraction images. Herein, (a) and (b) stand for the control and 90-shocked TiO_2 NPs; (c, d) stand for their corresponding zoomed-in portions of the electron diffraction images, respectively.

anatase and rutile phases exist with Ti^{4+} ions, and the band splitting energy difference in the Ti 2*p* states (Ti $2p_{3/2}$ and Ti $2p_{1/2}$) is 0.1 eV.[56,57] However, the XPS data can prove the existence of the crystallographic phases of the TiO_2 based on its core band positions of Ti and O as well as the valence band spectra, since the valence band spectra have various intensity profiles for both phases. For the control TiO_2 NPs, the peaks of the core Ti 2*p* bands are displayed in Figure 7a, which has two bands at 457.57 and 464.53 eV, and these two bands belong to the Ti $2p_{3/2}$ and Ti $2p_{1/2}$ states. At the 90-shocked condition, the obtained core Ti 2*p* bands are depicted in Figure 7b, wherein the bands are located at 463.27 and 463.22 eV. The observed slightly higher binding energy shift is probably owing to the rutile-to-anatase phase transition. As usual, oxygen vacancies are formed, which leads to the reduction of Ti ions from Ti^{4+} to Ti^{3+}, and the rutile-rich structures may have a few Ti^{3+} ions during the temperature-induced anatase-to-rutile phase transition in the crystal lattice.[58,59] The Ti^{3+} 2*p* state bands have occurred in the lower binding energy levels (456.1 and 461.94 eV for the Ti $2p_{3/2}$ and Ti $2p_{1/2}$ states of Ti^{3+}). In contrast, herein, the positive binding energy shift is found in the Ti 2*p* state bands at the 90-shocked condition, for which the available oxygen vacancies are reduced, whereby the Ti^{4+} ions are enhanced in the crystal lattice due to the formation of the anatase rich structure. Besides, the anatase has more than two times higher

https://doi.org/10.1021/acs.inorgchem.4c02723
Inorg. Chem. 2024, 63, 17043−17055

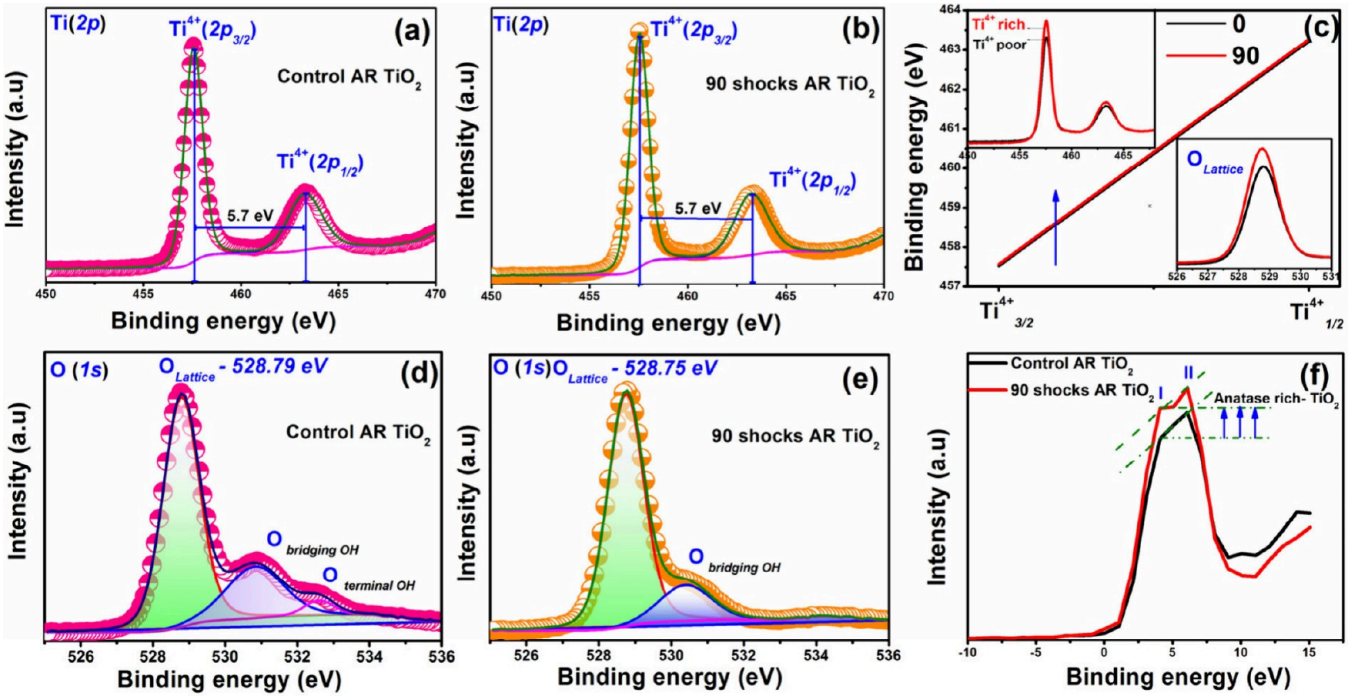

Figure 7. XPS spectra of the control and 90-shocked TiO_2 NPs. Herein, (a) and (b) represent the core Ti *2p* spectra of the control and 90-shocked TiO_2 NPs; (c) represents the binding energy shift of the Ti *2p* states for the control and 90 shocks (Inset: intensity comparative profiles of the Ti *2p* and O *1s* bands); (d) and (e) represent O *1s* spectra of the control and 90-shocked TiO_2 NPs; and (f) represents the valence band spectra of the control and 90-shocked TiO_2 NPs.

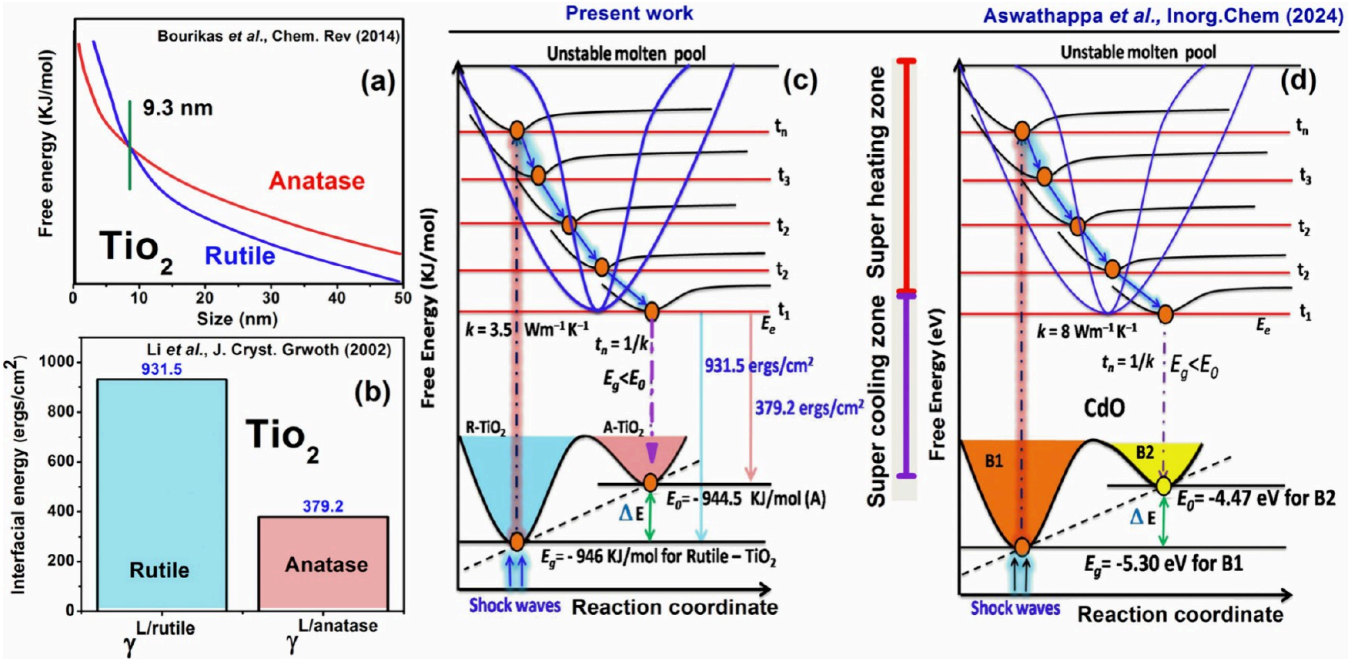

Figure 8. (a) Thermo-dynamical stability plot of the anatase and rutile TiO_2 with respect to their size (Reprinted Figure with permission from ref 10. Copyright (2004) American Chemical Society); (b) interfacial energy for the anatase and rutile TiO_2; (c) Thermal conductivity-driven energy diagrams of the rutile TiO_2, and (d) Thermal conductivity-driven energy diagrams of CdO NPs,[53] respectively; (Reproduced with permission from ref 53. Copyright (2004) by the American Chemical Society).

unit cell volume (136.2 $Å^3$) compared to the rutile cell volume (62 $Å^3$) such that the anatase structured particles have a larger number of Ti^{4+} and O^{2-} ions on the surface compared to rutile. In light of the higher concentration of the Ti^{4+} and O^{2-} on the surface, the intensities of the Ti *2p* and O *1s* bands are increased (Figure 7c).

In Figure 7d and e, the core O *1s* spectra are presented for the control and 90-shocked TiO_2 NPs. For the control sample, the lattice oxygen band appears at 528.79 eV, wherein the higher biding energy bands are due to the existing surface hydroxyl species.[60] At the 90-shocked condition, the O *1s* lattice oxygen band appears at 528.75 eV, in which a slightly

https://doi.org/10.1021/acs.inorgchem.4c02723
Inorg. Chem. 2024, 63, 17043−17055

lower binding energy shift is noticed with respect to the reduction of the available oxygen vacancies and the formation of the anatase-rich TiO_2 NPs.[56,57] In Figure 7f, the valence band XPS spectra of the control and 90-shocked TiO_2 NPs are presented, wherein a couple of peaks are witnessed at 4.09 and 6.01 eV. The intensity of a valence band spectrum depends on its orbital makeup. Since the TiO_2 phases have the same chemical composition, it is assumed here that the valence band spectrum has essentially the same orbital makeup (in this case consisting primarily of O 2p with some Ti 3d contribution), thereby having the same overall photoionization cross-section. Hence, the intensity of the fitted anatase component of a VB spectrum can be directly related to the amount of the anatase present within the sampling depth of the measurement. Therefore, it can be proposed that the XPS VB can efficiently extract quantitative phase information. As for the pure anatase phase, the lower binding energy band (Figure 7f, marked as I) has a higher intensity for the anatase and a lower intensity for the rutile.[61] At the 90-shocked condition, the enhancement of the intensity of the lower binding energy peak could be noticed, which could provide possible evidence for the rutile to anatase phase transition, as observed from XPS data.

Proposed Mechanism for the Rutile to Anatase Phase Transition. Based on the existing literature reports of the TiO_2, the thermodynamical stabilities for the rutile and anatase TiO_2 are expected to change with respect to the size of the particles.[10,62] For instance, in bulk particles, the rutile is considered a thermodynamically stable state and the anatase is considered a metastable state, whereas, in the case of ultrasmall size (below 10 nm) particles, the anatase becomes a thermodynamically stable phase and the rutile acts as the metastable state. The thermodynamical stability plot of the anatase and rutile TiO_2 with respect to their size is shown in Figure 8a. From the viewpoint of nucleation kinetics, the nucleation rate is determined by the interfacial energy between the liquid and solid as well as the thermodynamic driving force. The values of interfacial energy for the anatase and rutile of TiO_2 are 379.2 ergs/cm^2 and 931.5 ergs/cm^2, respectively (Figure 8b).[63] The values of the thermodynamic driving force (Gibbs free energy difference between the liquid and solid phases) for the anatase and rutile of TiO_2 are 0.85 J/m^2 and 1.5 J/m^2, respectively.[52] The molar free energies of the formation of the anatase and rutile phases are 2883.266 and 2889.406 kJ/mol, respectively. In addition to that, the surface energy of the anatase phase (1.275 J/m^2) is lower than that of the rutile phase (1.5 J/m^2).[52] Hence, the anatase phase has a critical radius smaller than that of the rutile particles. Due to the smaller particle size formation, the anatase has the first preference to be in the crystallized form in the molten state. A stability reversal hysteresis of the anatase−rutile transformation is because of the higher surface energy of rutile compared to anatase. Surface free energy is defined as the reversible work performed in creating a new unit surface area. Clean metal oxide surfaces are composed of ions with unsatisfied coordination, which means some atoms have unsatisfied electric charges. The more unsatisfied charges per unit surface area, the greater the work needed for creating the surface and, thus, the higher the surface energy. The rutile has more unsatisfied charges per unit surface area compared to anatase.[64] According to the critical energy for nucleation from melt or solution, the preferential nucleation is for the anatase instead of the rutile because of the lower interfacial energy between the anatase and liquid compared to the interfacial energy between the rutile and liquid.

Note that, under shocked conditions, lower thermal conductivity materials undergo the premelting processes by the shock wave-induced superheating effect which occurs within milliseconds of the transient time scale, and the premelting process of a test sample is represented as a prestate of the conventional melting process that enables homogeneous nucleation during sudden cooling whereby the final phase of the product is highly dependent on the interfacial energy between the liquid and solid state phases.[63] The superheating process occurs on the order of milliseconds, and after a few milliseconds, the sample undergoes rapid cooling; therefore, the surface becomes a region of low temperature, which initiates a significant dynamic recrystallization process.[53−55] In the present studies, the title sample has the anatase and rutile phases within it, such that the thermal conductivity values of the nanocrystalline anatase and rutile phases are 5.6 and 3.5 W m^{-1} K^{-1}, respectively.[65,66] The thermal expansion values of the anatase and rutile phases are 24.9×10^{-6} K^{-1} and 28.6×10^{-6} K^{-1}, respectively. Note that the rutile particles have higher thermal expansion ability compared to the anatase particles, which facilitates the fast-melting process and easy formation of the molten state during the superheating process.

At the 90-shocked condition, the rutile particles experience significant shock wave-induced superheating effects because of their slightly lower thermal transport ability, which facilitates the initiation of the premelting process. However, in the case of acoustic shock experiments, the shock pulse duration is considerably longer compared to the laser shock wave propagation time scale.[54,55] Because of this longer period, the local heating of the samples may take place over time scales on the order of milliseconds. This sustained slow heat propagation can allow the required latent heat to melt the samples. After the shock wave propagation, the test sample experiences a sudden cooling effect, and during such a process, the conversion of the molten state (liquid-like state) to solid state takes place. Note that, from the liquid-to-solid conversion of TiO_2, the most preferable phase is anatase due to its lower interfacial energy.[37−39,63] Moreover, in such a faster cooling time scale, the particles do not have time to make bigger grains (the critical nucleus size of rutile is much higher than that of anatase), and hence, the liquid-like particles are suddenly solidified with lower size particles, which restrict the rutile-to-rutile or anatase-to-rutile transitions; thereby, the rutile-to-anatase transition occurred. In addition to that, the shock wave-induced super heating occurs with the millisecond time scale and after a few milliseconds, the cooling process occurs,[67−71] and hence, at such a faster cooling rate, the atoms cannot find the required lowest energy sites in the lattice, whereby they crystallize at the possible highest energy sites such that the particles crystallize in the anatase phase.

Furthermore, according to ligand field theory, in a solution of the Ti (IV) ions exist 6-fold coordinated structural units (TiO_6), which undergo condensation to become the octahedra that bond via corner- and edge-sharing to form the final crystal structure. In the rutile form, TiO_6 octahedra link by sharing an edge along the *c*-axis to form chains that are interlinked by sharing corner oxygen atoms, whereas in the anatase, there is only edge sharing. Thus, the formation of anatase is highly preferable because of the less complex structure. Based on the above-mentioned perspective, anatase formation is highly favorable from the molten state due to the lower surface

https://doi.org/10.1021/acs.inorgchem.4c02723
Inorg. Chem. 2024, 63, 17043−17055

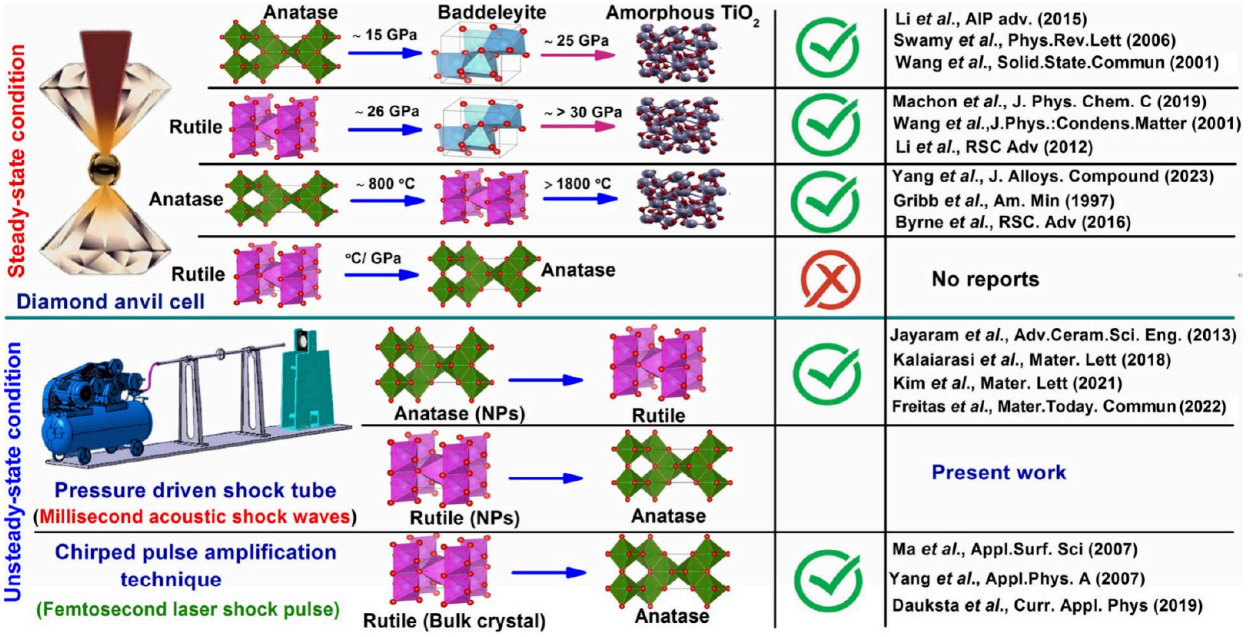

Figure 9. Structural transition path of TiO_2 under steady state (diamond anvil cell) and unsteady conditions (acoustic shock waves and femtosecond laser shock waves).

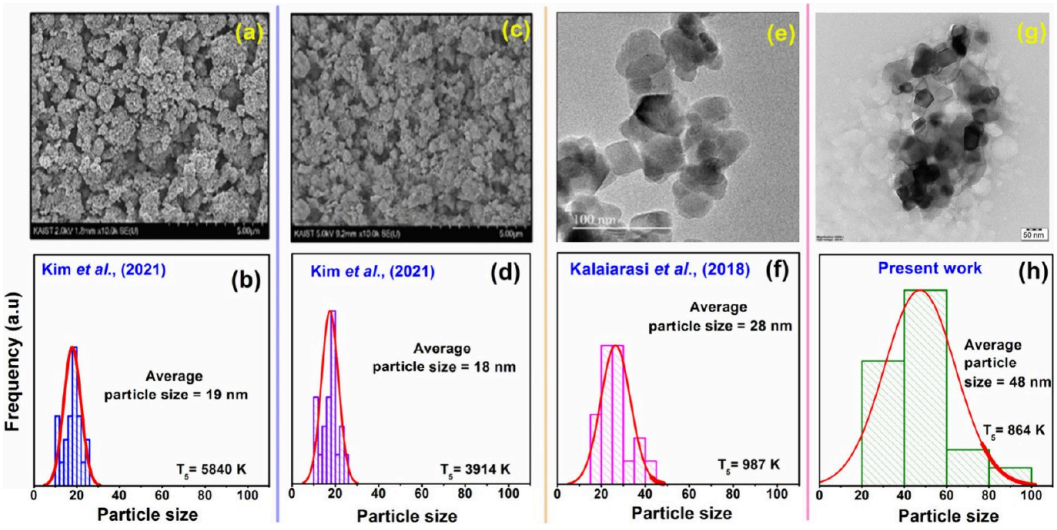

Figure 10. TEM images and particle size histogram profiles for the previously published shock wave-induced anatase to rutile phase transitions of TiO_2 (a, b)[43] (c, d)[43] (e, f)[45] (Reprinted figure with permission from ref.[43,43,45] Copyright (2021) by the Elsevier,[43] Copyright (2021) by the Elsevier,[43] and Copyright (2018) by the Elsevier,[45] (g, h) present work.

energy and lower critical size nucleus compared to rutile. Li et al. reported the solidification of the TiO_2 from melting and under a faster cooling rate, wherein the anatase nucleates are directly formed from the melt below 2057 K.[63] This result agrees with the current experimental observation that anatase is formed in a rapid cooling process. We propose a new mechanism to explain the rutile-to-anatase phase transition by acoustic shock waves which is based on the thermal conductivity of TiO_2.

Based on the previous results, it is found that materials of lower thermal conductivity undergo structural transitions.[53] In contrast, materials of higher thermal conductivity do not experience any structural transitions under shocked conditions.[67] To optimize this relation, it is considered that the value of the thermal conductivity of a material is inversely proportional to the molten pool width. If the thermal conductivity is low, under shocked conditions, the material can achieve the molten state, and during cooling conditions, it can crystallize in a different crystal structure. Assuming the width of the shock wave-induced unstable molten pool, it is divided by several time channels (t_n) at the unit volume, which means that the larger width molten pool has a greater number of time channels ($t_n = 1/k$) and vice versa for the lower width molten pool. The cooling time of the materials depends upon the value of the thermal conductivity and thermal diffusivity. If the thermal conductivity is high, the number of time channels in the molten width is much less and vice versa for the lower thermal conductivity materials.

Note that materials with low thermal transport can undergo a significant premelting process under shocked conditions,

https://doi.org/10.1021/acs.inorgchem.4c02723
Inorg. Chem. 2024, 63, 17043−17055

such that they have a greater number of time channels in the molten pool due to their larger width, and the atoms reach a lower energy state during the cooling process. When the atoms reach a lower energy state during the cooling process, they cannot find the lowest energy sites due to insufficient time (fast cooling process), and instantly, they can choose higher energy sites to crystallize, resulting in the structural transitions observed from rutile to anatase. The energy diagrams of Figure 8c highlight the acoustic shock wave-induced structural transitions based on the dynamic recrystallization process enabled by the thermal conductivity (k) of the test samples. The CdO NPs have undergone the structural transition from a lower energy state (B1) to a higher energy state (B2) under shocked conditions (Figure 8d).[53] The higher thermal conductivity materials such as ZnO,[67] MgO, Al_2O_3, graphite, and graphene do not undergo any kind of structural transitions under shocked conditions; however, the MgO, graphite, and graphene results are not discussed herein.

In a typical temperature- and pressure-induced phase transition on TiO_2, the anatase-to-rutile,[27,28] the anatase-to-baddeleyite,[20] and the rutile-to-baddeleyite[19] transitions are the allowed transition paths, whereas the rutile-to-anatase phase transition is conventionally not possible because of the absence of superheating and cooling processes, and the corresponding schematic diagram is presented in Figure 9. However, laser shock waves and acoustic shock waves could provide the transition path between the rutile and anatase TiO_2.[37−39]

Why Has the Rutile-to-Anatase Transition Occurred Rather Than the Anatase-to-Rutile Transition? According to the previous reports of acoustic shock wave effects on TiO_2 NPs,[42−44] the anatase-to-rutile transition is highly known, easy, and a possible transition path, such that the transition is proposed based on the same dynamic recrystallization mechanism.[42−44] Now, one common question may arise; for instance, in the present work, the test sample has anatase and rutile phases whereby the anatase particles should be converted into the rutile phase under shocked conditions, and at the final stage, the rutile phase content of the particles will be increased. But, why has it not happened? Herein, two possible reasons are considered for the observed rutile-to-anatase transition. First, in the previous reports, the initial particle size is lower[43,44] than that of the preset work (Figure 10). According to the thermal stability theoretical calculation profiles with respect to their size, anatase is considered as a lower energy state while the particle size is lower than the 10 nm, while under shocked conditions, thereby the atoms are crystallized in the higher energy sites such that the anatase-to-rutile phase transition has occurred. In refs 43 and 45, the initial particle sizes are slightly higher than the theoretical critical size of the inverse stability of TiO_2. However, in experimental conditions, the critical size of the inverse stability can be slightly increased based on the particle shapes, purity, surface roughness, thermal conductivity, and so on. Second, the thermal conductivity of the rutile particles is lower than that of the anatase phase, such that, under shocked conditions, the sample can undergo a high degree of premelting process, thereby creating a high degree of molten state based on the superheating effect. In such cases, the anatase phase has a higher possibility to crystallize during the sudden cooling process.

CONCLUSIONS

In the present work, we report the unconventional thermodynamic rutile-to-anatase phase transition in TiO_2 NPs under acoustic shocked conditions, and the results have been evaluated by Raman spectroscopic, DSC, SEM, TEM and XPS techniques. The Raman spectroscopy results evidently demonstrate the intensity reduction of the characteristic rutile Raman bands such as 447 (E_g) and 610 cm^{-1} (A_{1g}) at the 90-shocked condition. By the DSC technique, the anatase-to-rutile transition is witnessed, such that the exothermic peak intensity is found to have increased, which provides robust evidence for the 90-shocked sample possessing a higher number of anatase particles. Most importantly, the particle sizes have significantly reduced at the 90-shocked condition, which is one of the strong pieces of evidence for the proposed phase transition. Furthermore, the acoustic shock wave-induced phase transition of the sample from those of our acquired electron diffraction and XPS results is also illustrated in detail. According to the thermal conductivity values and shock wave-induced melting concepts, this is the first time that a novel mechanism was put forward to reasonably explain the occurrence of the rutile-to-anatase phase transition. In light of the lower interfacial energy ($\gamma^{L/A}$) of the anatase phase compared to the rutile phase, the R−A transition occurs under shocked conditions. We strongly believe that the present work can provide a new platform to understand the crystallization concepts of the TiO_2 NPs under extreme conditions, especially for the rutile-to-anatase phase transition of nano and bulk size particles. In addition to that, it can offer a new pathway to initiate studies on the unconventional thermodynamic structural transition arising out of tabletop shock tube experiments whereby the effectiveness of tabletop shock tubes over conventional high-pressure tools such as a diamond anvil cell can be affirmed. Materials such as $MoSi_2$ and Al_2O_3 can undergo phase transitions from the stable state to metastable states during a fast melting and solidification process such as that of TiO_2. These materials are alternative candidates to examine such unconventional phase transition processes under shocked conditions.

ASSOCIATED CONTENT

Supporting Information

The Supporting Information is available free of charge at https://pubs.acs.org/doi/10.1021/acs.inorgchem.4c02723.

Additional experimental details of the shock wave loading procedure; analytical instrument details, and survey XPS spectra of the control and 90-shocked TiO_2 NPs (PDF)

AUTHOR INFORMATION

Corresponding Author

Lidong Dai − *Key Laboratory of High-Temperature and High-Pressure Study of the Earth's Interior, Institute of Geochemistry, Chinese Academy of Sciences, Guiyang, Guizhou 550081, China;* orcid.org/0000-0002-9081-765X; Email: dailidong@vip.gyig.ac.cn

Authors

Sivakumar Aswathappa − *Key Laboratory of High-Temperature and High-Pressure Study of the Earth's Interior, Institute of Geochemistry, Chinese Academy of Sciences, Guiyang, Guizhou 550081, China*

https://doi.org/10.1021/acs.inorgchem.4c02723
Inorg. Chem. 2024, 63, 17043−17055

Sahaya Jude Dhas Sathiyadhas − *Saveetha School of Engineering, Saveetha Institute of Medical and Technical Sciences, Saveetha University, Chennai, Tamil Nadu 602105, India*

Raju Suresh Kumar − *Department of Chemistry, College of Science, King Saud University, Riyadh 11451, Saudi Arabia;* orcid.org/0000-0003-3754-4223

Mowlika Varadhappa Reddy − *Department of Physics, St Joseph's College of Arts and Science for Women, Hosur, Tamilnadu 635 126, India*

Complete contact information is available at: https://pubs.acs.org/10.1021/acs.inorgchem.4c02723

Author Contributions

L.D. conceived the idea and led the project. S.A. performed the acoustic shock wave measurements. L.D., S.A, S.J.D.S., R.S.K., and M.V.R. contributed to the analysis, interpretation, and discussion of results. S.A. wrote the manuscript with the help of all the authors. All the authors commented on the final manuscript. L.D. supervised the project.

Notes

The authors declare no competing financial interest.

■ ACKNOWLEDGMENTS

The authors thank the NSF of China (42072055). This project was supported by the Researchers Supporting Project number (RSP2024R142), King Saud University, Riyadh, Saudi Arabia.

■ REFERENCES

(1) Schneider, J.; Matsuoka, M.; Takeuchi, M.; Zhang, J.; Horiuchi, J.; Anpo, M.; Bahnemann, D. W. Understanding TiO_2 photocatalysis: mechanisms and materials. *Chem. Rev.* **2014**, *114*, 9919−9986.

(2) Li, K.; Wang, J.; Oganov, A. R. High-pressure phase diagram of the Ti-O system. *J. Phys. Chem. Lett.* **2021**, *12*, 5486−5493.

(3) Popescu, C.; Sans, J. A.; Errandonea, D.; Segura, A.; Villanueva, R.; Sapina, F. Compressibility and structural stability of nanocrystalline TiO_2 anatase synthesized from freeze-dried precursors. *Inorg. Chem.* **2014**, *53*, 11598−11603.

(4) Zhong, X.; Yang, L.; Qu, X.; Wang, Y.; Yang, J.; Ma, Y. Crystal structures and electronic properties of oxygen-rich titanium oxides at high pressure. *Inorg. Chem.* **2018**, *57*, 3254−3260.

(5) Dubrovinskaia, N. A.; Dubrovinsky, L. S.; Ahuja, R.; Prokopenko, V. B.; Dmitriev, V.; Weber, H. P.; Osorio-Guillen, J.; Johansson, M. B. Experimental and theoretical identification of a new high-pressure TiO_2 polymorph. *Phys. Rev. Lett.* **2001**, *87*, 275501.

(6) Zhu, T.; Gao, S. P. The stability, electronic structure, and optical property of TiO_2 polymorphs. *J. Phys. Chem. C* **2014**, *118*, 11385−11396.

(7) Muscat, J.; Swamy, V.; Harrison, N. M. First-principles calculations of the phase stability of TiO_2. *Phys. Rev. B* **2002**, *65*, 224112.

(8) Liu, J.; Yu, Y.; He, H.; Jin, X.; Xu, K. Photocatalytic activity of shock-treated TiO_2 powder. *Mater. Res. Bull.* **2000**, *35*, 377−382.

(9) Lee, J. G.; Pickard, C. J.; Cheng, B. High-pressure phase behaviors of titanium dioxide revealed by a Δ-learning potential. *J. Chem. Phys.* **2022**, *156*, 074106.

(10) Bourikas, K.; Kordulis, C.; Lycourghiotis, A. Titanium dioxide (anatase and rutile): surface chemistry, liquid− solid interface chemistry, and scientific synthesis of supported catalysts. *Chem. Rev.* **2014**, *114*, 9754−9823.

(11) Barnard, A. S.; Zapol, P. Effects of particle morphology and surface hydrogenation on the phase stability of TiO_2. *Phys. Rev. B* **2004**, *70*, 235403.

(12) Wang, X.; Li, Z.; Shi, Z.; Yu, Y. One-dimensional titanium dioxide nanomaterials: nanowires, nanorods, and nanobelts. *Chem. Rev.* **2014**, *114*, 9346−9384.

(13) Noman, M. T.; Ashraf, M. A.; Ali, A. Synthesis and applications of nano-TiO_2: a review. *Environ. Sci. Pollut. Res.* **2019**, *26*, 3262−3291.

(14) Sekiya, T.; Ohta, S.; Kamei, S.; Hanakawa, M.; Kurita, S. Raman spectroscopy and phase transition of anatase TiO_2 under high pressure. *J. Phys. Chem. Solids.* **2001**, *62*, 717−721.

(15) Lu, X.; Gao, S.; Wu, P.; Zhang, Z.; Zhang, L.; Li, X.; Qin, X. *In-situ* high-pressure Raman spectroscopic, single-crystal X-ray diffraction, and FTIR investigations of rutile and TiO_2-II. *Min.* **2023**, *13*, 703.

(16) Kusaba, K.; Kikuchi, M.; Fukuoka, K.; Syono, Y. Anisotropic phase transition of rutile under shock compression. *Phys. Chem. Min.* **1988**, *15*, 238−5245.

(17) Mashimo, T.; Nagayama, K.; Sawaoka, A. Anisotropic elastic limits and phase transitions of rutile phase TiO_2 under shock compression. *J. Appl. Phys.* **1983**, *54*, 5043−5048.

(18) Duwal, S.; Root, S.; Farfan, B.; Reinhart, W.; Alexander, C. S. Dynamic compression of TiO_2 to 221 GPa. *J. Appl. Phys.* **2021**, *130*, 165903.

(19) Li, Q.; Liu, R.; Liu, B.; Wang, L.; Wang, K.; Li, D.; Zou, B.; Cui, T.; Liu, J.; Chen, Z.; Yang, K. Stability and phase transition of nanoporous rutile TiO_2 under high pressure. *RSC Adv.* **2012**, *2*, 9052−9057.

(20) Wang, Z.; Saxena, S. K.; Pischedda, V.; Liermann, H. P.; Zha, C. S. X-ray diffraction study on pressure-induced phase transformations in nanocrystalline anatase/rutile (TiO_2). *J. Phys.: Condens. Matter.* **2001**, *13*, 8317−8323.

(21) Li, Q.; Cheng, B.; Yang, X.; Liu, R.; Liu, B.; Liu, J.; Chen, Z.; Zou, B.; Cui, T.; Liu, B. Morphology-tuned phase transitions of anatase TiO_2 nanowires under high pressure. *J. Phys. Chem. C* **2013**, *117*, 8516−8521.

(22) Li, Q.; Liu, R.; Wang, T.; Xu, K.; Dong, Q.; Liu, B.; Liu, J.; Liu, B. High pressure synthesis of amorphous TiO_2 nanotubes. *AIP Adv.* **2015**, *5*, 097128.

(23) Swamy, V.; Kuznetsov, A.; Dubrovinsky, L. S.; McMillan, P. F.; Prakapenka, V. B.; Shen, G.; Muddle, B. C. Size-dependent pressure-induced amorphization in nanoscale TiO_2. *Phys. Rev. Lett.* **2006**, *96*, 135702.

(24) Swamy, V.; Kuznetsov, A.; Dubrovinsky, L. S.; Caruso, R. A.; Shchukin, D. G.; Muddle, B. C. Finite-size and pressure effects on the Raman spectrum of nanocrystalline anatase TiO_2. *Phys. Rev. B* **2005**, *71*, 184302.

(25) Hearne, G. R.; Zhao, J.; Dawe, A. M.; Pischedda, V.; Maaza, M.; Nieuwoudt, M. K.; Kibasomba, P.; Nemraoui, O.; Comins, J. D.; Witcomb, M. J. Effect of grain size on structural transitions in anatase TiO_2: A Raman spectroscopy study at high pressure. *Phys. Rev. B* **2004**, *70*, 134102.

(26) Arlt, T.; Bermejo, M.; Blanco, M. A.; Gerward, L.; Jiang, J. Z.; Olsen, J. S.; Recio, J. M. High-pressure polymorphs of anatase TiO_2. *Phys. Rev. B* **2000**, *61*, 14414−14419.

(27) Byrne, C.; Fagan, R.; Hinder, S.; McCormack, D. E.; Pillai, S. C. New approach of modifying the anatase to rutile transition temperature in TiO_2 photocatalysts. *RSC Adv.* **2016**, *6*, 95232.

(28) Zhu, X.; Han, S.; Feng, W.; Kong, Q.; Dong, Z.; Wang, C.; Lei, J.; Yi, Q. The effect of heat treatment on the anatase-rutile phase transformation and photocatalytic activity of Sn-doped TiO_2 nanomaterials. *RSC Adv.* **2018**, *8*, 14249.

(29) Karunadasa, K. S. P.; Manoratne, C. H. Microstructural view of anatase to rutile phase transformation examined by in-situ high-temperature X-ray powder diffraction. *J. Solid. State. Chem.* **2022**, *314*, 123377.

(30) Hanaor, D. A. H.; Sorrell, C. C. Review of the anatase to rutile phase transformation. *J. Mater. Sci.* **2011**, *46*, 855−874.

(31) Luo, Y.; Benali, A.; Shulenburger, L.; Krogel, J. T.; Heinonen, O.; Kent, P. C. R. Phase stability of TiO_2 polymorphs from diffusion quantum monte Carlo. *New. J. Phys.* **2016**, *18*, 113049.

(32) Medvids, A.; Varnagiris, S.; Letko, E.; Milcius, D.; Grase, L.; Gaidukovs, S.; Mychko, A.; Pludons, A.; Onufrijevs, P.; Mimura, H. Phase transformation from rutile to anatase with oxygen ion dose in the TiO_2 layer formed on a Ti substrate. *Mater. Sci. Semicond. Process.* **2020**, *106*, 104776.
(33) Ruzybayev, I.; Shah, S. I. The role of oxygen pressure in nitrogen and carbon co-doped TiO_2 thin films prepared by pulsed laser deposition method. *Surf. Coat. Technol.* **2014**, *241*, 148−153.
(34) Kittaka, S.; Matsuno, K.; Takahara, S. Transformation of ultrafine titanium dioxide particles from rutile to anatase at negatively charged colloid surfaces. *J. Solid. State. Chem.* **1997**, *132*, 447−450.
(35) Bhosale, R.; Hyam, R.; Dhanya, P.; Ogale, S. Chlorate ion mediated rutile to anatase reverse phase transformation in the TiO_2 nanosystem. *Dalton Trans.* **2011**, *40*, 11374.
(36) Breeson, A. C.; Sankar, G.; Goh, G. K. L.; Palgrave, R. G. Rutile to Anatase phase transition induced by N doping in highly oriented TiO_2 films. *Phys. Chem. Chem. Phys.* **2016**, *18*, 24722−24728.
(37) Ma, H. L.; Yang, J. Y.; Dai, Y.; Zhang, Y. B.; Lu, B.; Ma, G. H. Raman study of phase transformation of TiO_2 rutile single crystal irradiated by infrared femtosecond laser. *Appl. Surf. Sci.* **2007**, *253*, 7497−7500.
(38) Yang, J. Y.; Ma, H. L.; Ma, G. H.; Lu, B.; Ma, H. Phase transformation at the surface of TiO_2 single crystal irradiated by femtosecond laser pulse. *Appl. Phys. A: Mater. Sci. Process.* **2007**, *88*, 801−804.
(39) Dauksta, E.; Medvids, A.; Onufrijevs, P.; Shimomura, M.; Fukuda, Y.; Murakami, K. Laser-induced crystalline phase transition from rutile to anatase of niobium doped TiO_2. *Curr. Appl. Phys.* **2019**, *19*, 351−355.
(40) Aswathappa, S.; Soundarya, S.; Sathiyadhas, S. J. D.; Bharathi, K. K.; Dhas, S. A. M. B. Shock wave driven solid state phase transformation of Co_3O_4 to CoO nanoparticles. *J. Phys. Chem. C* **2020**, *124*, 10755−10763.
(41) Aswathappa, S.; Rita, A.; Sathiyadhas, S. J. D.; Reddy, K. P. J.; Kumar, R. S.; Almansour, A. I.; Chakraborty, S.; Moovendaran, K.; Sridhar, J.; Martin Britto Dhas, S. A. Dynamic shock wave driven simultaneous crystallographic and molecular switching between α-Fe_2O_3 and Fe_3O_4 nanoparticles - a new finding. *Dalton Trans.* **2022**, *51*, 9159−9166.
(42) Jayaram, V.; Preetam, S.; Reddy, K. P. J. Study of anatase TiO_2 in the presence of N_2 under shock dynamic loading in a free piston driven shock tube. *Adv. Ceram. Sci. Eng.* **2013**, *2*, 40−46.
(43) Kim, I.; Shim, H.; Kim, Y.; Park, G. Effect of shock-heated flow on morphological and structural properties of anatase TiO_2 nanoparticles. *Mater. Lett.* **2021**, *294*, 129793.
(44) Slama de Freitas, A. L.; Subburaj, J.; Navarro, J. C.; Khan, H. A.; Kashif, T. A.; Hakimov, K.; Ruiz-Martinez, J.; Farooq, A. Shockwave impact on the stability of anatase titania nanoparticles. *Mater. Today. Commun.* **2022**, *32*, 104031.
(45) Kalaiarasi, S.; Aswathappa, S.; Dhas, S. A. M. B.; Jose, M. Shock wave induced anatase to rutile TiO_2 phase transition using pressure driven shock tube. *Mater. Lett.* **2018**, *219*, 72−75.
(46) Aswathappa, S.; Kalaiarasi, S.; Dhas, S. S. S.; Sivaprakash, P.; Arumugam, S.; Jose, M.; Martin Britto Dhas, S. A. Comparative assessment of crystallographic phase stability of anatase and rutile TiO_2 at dynamic shock wave loaded conditions. *J. Inorg. Organomet. Polym.* **2022**, *32*, 967−972.
(47) Aswathappa, A.; Kalaiarasi, S.; Dhas, S. S. J.; Almansour, A. I.; Kumar, R. S.; Arumugam, N.; Dhas, S. A. M. B. Assessment of shock wave resistance on brookite TiO_2. *J. Mater. Sci: Mater. Electron.* **2021**, *32*, 15134−15142.
(48) Perego, C.; Revel, R.; Durupthy, O.; Cassaignon, S.; Jolivet, J. P. Thermal stability of TiO_2-anatase: Impact of nanoparticles morphology on kinetic phase transformation. *Solid. State. Sci.* **2010**, *12*, 989−995.
(49) Kalaiarasi, S.; Martin Britto Dhas, S. A.; Jose, M.; Jerome Das, S. Thermo analytical study of phase transformation of TiO_2 nanoparticles prepared using mono and di α-hydroxy acid water-soluble precursor by hydrothermal technique. *Phase. Transit.* **2020**, *93*, 722−732.
(50) da Silva, A. L.; Hotza, D.; Castro, R. H.R. Surface energy effects on the stability of anatase and rutile nanocrystals: A predictive diagram for Nb_2O_5-doped-TiO_2. *Appl. Surf. Sci.* **2017**, *393*, 103−109.
(51) Reidy, D. J.; Holmes, J. D.; Morris, M. A. The critical size mechanism for the anatase to rutile transformation in TiO_2 and doped-TiO_2. *J. Eur. Ceram. Soc.* **2006**, *26*, 1527−1534.
(52) Gribb, A. A.; Banfield, J. F. Particle size effects on transformation kinetics and phase stability in nanocrystalline TiO_2. *Am. Mineral.* **1997**, *82*, 717−728.
(53) Aswathappa, S.; Dai, L.; Jude Dhas, S. S.; Dhas, S. A. M. B.; Laha, S.; Kumar, R. S.; Almansour, A. I. Acoustic shock wave-induced solid-state fusion of nanoparticles: a case study of the conversion of one-dimensional rod shape into three-dimensional honeycomb nanostructures of CdO for high performance energy storage materials. *Inorg. Chem.* **2024**, *63*, 576−592.
(54) Aswathappa, S.; Dai, L.; Dhas, S. S. S.; Dhas, S. A. M. B.; Eniya, P.; Suresh Kumar, R.; Almansour, A. I. Synthesis of crystalline graphite from disordered graphite by acoustic shock waves: Hot-spot nucleation approach. *Appl. Surf. Sci.* **2024**, *655*, 159632.
(55) Aswathappa, S.; Dai, L.; Jude Dhas, S. S.; Dhas, S. A. M. B.; Palaniyasan, E.; Kumar, R. S.; Almansour, A. I. Experimental evidence of acoustic shock wave-induced dynamic recrystallization: a case study on ammonium sulfate. *Cryst. Growth Des.* **2024**, *24*, 491−498.
(56) Byrne, C.; Moran, L.; Hermosilla, D.; Merayo, N.; Blanco, A.; Rhatigan, S.; Hinder, S.; Ganguly, P.; Nolan, M.; Pillai, S. C. Effect of Cu doping on the anatase-to-rutile phase transition in TiO_2 photocatalysts: theory and experiments. *Appl. Catal., B* **2019**, *246*, 266−276.
(57) Padmini, M.; Balaganapathi, T.; Thilakan, P. Mesoporous rutile TiO_2: Synthesis, characterization and photocatalytic performance studies. *Mater. Res. Bull.* **2021**, *144*, 111480.
(58) Etacheri, V.; Seery, M. K.; Hinder, S. S.; Pillai, S. C. Oxygen rich titania: a dopant free, high temperature stable, and visible-light active anatase photocatalyst. *Adv. Funct. Mater.* **2011**, *21*, 3744−3752.
(59) Mathew, S.; Ganguly, P.; Rhatigan, S.; Kumaravel, V.; Byrne, C.; Hinder, S. J.; Bartlett, J.; Nolan, M.; Pillai, S. C. Cu-doped TiO_2: visible light assisted photocatalytic antimicrobial activity. *Appl. Sci.* **2018**, *8*, 2067.
(60) Tan, X.; Fan, Q.; Wang, X.; Grambow, B. Eu (III) Sorption to TiO_2 (Anatase and Rutile): Batch, XPS, and EXAFS Studies. *Environ. Sci. Technol.* **2009**, *43*, 3115−3121.
(61) Challagulla, S.; Tarafder, K.; Ganesan, R.; Roy, S. Structure sensitive photocatalytic reduction of nitroarenes over TiO_2. *Sci. Rep.* **2017**, *7*, 8783.
(62) Barnard, A. S.; Zapol, P. Effects of particle morphology and surface hydrogenation on the phase stability of TiO_2. *Phys. Rev. B* **2004**, *70*, 235403.
(63) Li, Y.; Ishigaki, T. Thermodynamic analysis of nucleation of anatase and rutile from TiO_2 melt. *J. Cryst. Growth.* **2002**, *242*, 511−516.
(64) Zhang, H.; Banfield, J. F. Thermodynamic analysis of phase stability of nanocrystalline titania. *J. Mater. Chem.* **1998**, *8*, 2073−2076.
(65) Feng, X.; Huang, X.; Wang, X. Thermal conductivity and secondary porosity of single anatase TiO_2 nanowire. *Nanotechnology.* **2012**, *23*, 185701.
(66) Verchere, A.; Pailhes, S.; Le Floch, S.; Cottrino, S.; Debord, R.; Fantozzi, G.; Misra, S.; Candolfi, C.; Lenoir, B.; Daniele, S.; Mishra, S. Optimum in the thermoelectric efficiency of nanostructured Nb-doped TiO_2 ceramics: from polarons to Nb-Nb dimers. *Phys. Chem. Chem. Phys.* **2020**, *22*, 13008.
(67) Jayaram, V.; Preetam, S.; Reddy, K. P. J. Experimental investigation of nano ceramic material interaction with high enthalpy argon under shock dynamic loading. *Appl. Mech. Mater.* **2011**, *83*, 66−72.

https://doi.org/10.1021/acs.inorgchem.4c02723
Inorg. Chem. 2024, 63, 17043−17055

(68) Vishakantaiah, J.; Ranjith, R.; Bera, P. Non-catalytic behavior of SiO_2 fine Powders in presence of strong shock waves for aerospace applications. *J. Mater. Sci. Appl.* **2018**, *4*, 37−46.
(69) Vishakantaiah, J.; Reddy, K. P. J. Catalytic effect of CeO_2-stabilized ZrO_2 ceramics with strong shock-heated mono- and di-atomic gases. *J. Am. Ceram. Soc.* **2016**, *99*, 4128−4136.
(70) Jayaram, V.; Gupta, A.; Reddy, K. P. J. Investigation of strong shock wave interactions with CeO_2 ceramic. *J. Adv. Ceram.* **2014**, *3*, 297−305.
(71) Aswathappa, S.; Victor, C.; Nayak, M. M.; Dhas, S. A. M. B. Structural, optical, and morphological stability of ZnO nano rods under shock wave loading conditions. *Mater. Res. Express.* **2019**, *6*, 045031.

https://doi.org/10.1021/acs.inorgchem.4c02723
Inorg. Chem. 2024, 63, 17043−17055